INTERNATIONAL JOURNAL OF AUTOMOTIVE AND MECHANICAL ENGINEERING
ISSN: 2229-8649 e-ISSN: 2180-1606
VOL. 20, ISSUE 3, 2023, 10635–10648
DOI: https://doi.org/10.15282/ijame.20.3.2023.07.0821

اونيۏرسيتي مليسيا ڤهڠ
UNIVERSITI MALAYSIA PAHANG

RESEARCH ARTICLE

Mechanical Analysis and Constitutive Modeling of Nonlinear Behavior of Silver-based Conductive Ink

S. Zulfiqar[1], A.A. Saad[1,*], Z. Ahmad[2] and Z. Bachok[1]

[1]School of Mechanical Engineering, Universiti Sains Malaysia, 14300 Nibong Tebal, Pulau Pinang, Malaysia
[2]School of Materials & Mineral Resources Engineering, Universiti Sains Malaysia, 14300 Nibong Tebal, Pulau Pinang, Malaysia

ABSTRACT - Stretchable electronic devices are progressively deployed in many applications of mechanical, electrical, and biomedical engineering. These circuits are made of stretchable and flexible substrates, as well as conductive ink and various electronic components. The choice of components and layouts for the substrate and conductive ink can regulate the stretchability of stretchable circuits. On top of that, the substance utilized to create the conductive ink must have high electrical conductivity and strong adherence to the substrate in order to produce a high-quality stretchable printed circuit. Thus, this study focused on the development of stretchable conductive ink using silver powder as a conductive filler and PDMS-OH as a binder. The mechanical properties of the synthesized ink were investigated via a simple uniaxial tensile testing method and nanoindentation technique, respectively. Accordingly, the modulus of elasticity, tensile stress and yield stress of the ink were obtained as 5.72 MPa, 1.195 MPa, and 0.86 MPa, congruently at 137% strain before undergoing failure. The experimental stress-strain data was then employed on the elastic-plastic constitutive model to investigate the elastomeric properties of the ink as it is an alternative method of lengthy and expensive procedures of validating different polymers. Moreover, the hardness and reduced modulus of the ink were evaluated by the nanoindentation method using a 5 mN maximum load with 0.5 mN/s loading/unloading rate and 2 secs holding time. Consequently, the hardness and reduced modulus values were obtained as 1.45 MPa and 34.53 MPa, respectively. These values were further validated by the Oliver-Pharr method and were in good agreement.

ARTICLE HISTORY

Received	:	21st Nov 2022
Revised	:	10th May 2023
Accepted	:	31st May 2023
Published	:	26th Sept 2023

KEYWORDS
Conductive ink;
Tensile testing;
Elastic-plastic modelling;
FE analysis;
Nanoindentation test

1.0 INTRODUCTION

In the last few decades, stretchable and flexible electronic devices are playing an excellent role in various mechanical and electrical applications like mechanical sensors [1], actuators, microfluidic circuits [2], robotics [3], and electronic devices [4,5]. These devices are composed of stretchable substrate, conductive ink and electronic components like LED. Conductive ink is the most important and primary part of any electronic system that can be designed or fabricated into a certain geometry to get the desired stretchability. The conductive inks are used in potential electronic applications such as LED display [6,7], touch panels [8], health monitoring devices [9], smart sensors [10], transistor arrays [11], artificial electronic skins [12,13] and so on.

Several researches have been carried out on the development of different conductive inks in which different types of conductive fillers and elastomers have been utilized [14–21]. These conductive fillers include carbon-based conductors (like single-walled carbon nanotubes (SWCNTs), graphene, graphite, carbon fiber), metal-based (gold (Au), silver (Ag), copper (Cu), aluminum (Al)) and organic conductive polymers (PEDOT: PSS, PANi, polypyrrole (PPy)) [22]. In recent studies, silver is utilized as a conductive filler of various geometrical shapes and sizes like powder, wires, flakes and particles, in the formation of stretchable conductive ink because it possesses high electrical conductivity ($6.3 \times 10^7\ \Omega^{-1}\ m^{-1}$) [23–26] and remains conductive after atmospheric exposure than the other metallic fillers like copper and aluminum whose electrical conductivity decreases after reacting with oxygen [23,24]. Apart from the conductive filler, selection of the binder is also very important to produce the desired conductivity as it helps to connect the elements of conductive filler with each other. However, the most widely used binders are elastomers such as polydimethylsiloxane (PDMS) [14], polyurethanes (PU) [27], Ecoflex [28] and poly(styrene-butadiene-styrene) (SBS).

The reliability and strength of a material can be examined using several experimentation techniques. Among them, the most common and general method of calculating the mechanical strength of silver-based conductive is performing tensile testing on a universal tensile testing machine (UTM). Since the conductive ink is a polymeric composite, therefore, it possesses nonlinear stress-strain behavior during loading and unloading conditions [29–32]. It has been found from the literature that the polymer composites show nonlinear and inelastic behaviour in shearing and transverse compression conditions, while on the other hand, they behave elastically in the fibre direction before failure. It is assumed that the nonlinear behaviour of these composites only occur due to the brittle nature of the polymers which are used in making

*CORRESPONDING AUTHOR | A.A. Saad | ✉ azizsaad@usm.my

the polymeric composites and can be solved by continuum damage mechanics theory [33]. Thus, the convenient way of predicting the structural behavior of a composite is to impose an elastic-plastic model based on the macroscopic approach on the experimental data. The size and direction of the yield surface depend on the rules of isotropic and kinematic hardening, respectively. However, the simplest formation of plasticity models involves the linearity functions which are restricted to monotonic loading only. As a consequence, the elastic-plastic models help to solve the complex behavior of polymeric composites that depends on the strain rate [34], temperature [35], stress state [36], large deformations and plastic flow [37]. Though the mathematical equations of these constitutive models are obtained via plasticity theory which is based on the yield function criterion, plastic potential function or flow rule and hardening rule.

Apart from various mechanical tests like tension, compression, flexural, dynamic and impact, the consistency of polymeric composites in electrical, optical and mechanical areas can be predicted by considering the effect of size, different coatings on a small scale and the effect of modest inclusions. Due to this reason, large-scale mechanical tests are not applicable, and thus, a non-destructive, proficient and faster technique is used to explore the mechanical properties of the polymeric composites at the micro or nano level. This advanced technique is known as the nanoindentation technique, which fulfils all the limitations and has become a very popular method of finding mechanical properties under complex conditions with high resolution of different polymers and their composites [38,39]. The depth sensing indentation (DSI) or nanoindentation technique is widely used to extract the hardness and elastic properties of specimens with known geometry of indenters and material properties, as mentioned by Oliver-Pharr [40]. The commonly used indenters are pyramidal three-sided Berkovich and four-sided Vickers [41,42]. These indenters are treated as conical indenters with equivalent half angle α. The area-to-depth ratios of conical indenters are the same as that of pyramidal indenters.

Many researchers have used the nanoindentation method to investigate the mechanical properties of polymers and their composites [43–45]. These composites are tested to examine their elastic, elastic-plastic, visco-elastic and visco-plastic behavior depending on the requirement of the respective application [46–49]. Hence, the nanoindentation method is employed efficiently to study the mechanical changes that occur in polymeric composites [44–46]. Moreover, the mechanical properties of three types of carbon nanotube or carbon nanofiber-reinforced composites were examined using the nanoindentation technique by Lee et al. [50]. They compared the mechanical properties of neat epoxy with the nano-array reinforced epoxy at the nano-level. Jee and Lee [51] adopted the atomic force microscopy (AFM) nanoindentation method to measure the elastic modulus and hardness of several polymers. The ten different polymers were tested such as low density polyethylene (LDPE), polyvinyl alcohol (PVA), high density polyethylene (HDPE), ultra-high molecular weight polyethylene (UHMWPE), polyvinyl chloride (PVC), polycarbonate (PC), Nylone 6, poly (methyl methacrylate) (PMMA), polystyrene (PS) and polyacrylic acid (PAA). Similarly, Ferencz et al. [43] determined the mechanical properties of EPDM elastomer by atomic force microscopy nanoindentation (AFM) at various curing temperatures and crystallinity. The review of nanoindentation on different polymers was done by Diez-Pascual et al. [52], in which they used different nanofillers such as graphene, carbon nanotubes and nano clay to make the polymeric composites and examined their modulus of elasticity, hardness and creep values at small-scale. Also, the visco-elastic creep properties of soft materials were investigated by Zhang et al. [53] using different types of indenters in the nanoindentation method, while Goodarzi et al. [54] computed the visco-elastic properties of glass/epoxy composite by nanoindentation method and applied the experimental data on three-element Zener model for curve-fitting. In the same way, Wang et al. [55] studied the visco-elastic properties of different polymers by applying the experimental data from nanoindentation on the three-element Maxwell and visco-elastic contact models.

Based on the literature review, it is important to study the mechanical properties of polymers and their composites at the macro and micro levels for various engineering applications. The objective of this research is to examine the mechanical properties of silver-based ink by UTM and nanoindentation methods. At first, the ink was fabricated and tested uniaxially on UTM to determine its stress-strain behavior under large deformation. Since the silver ink contains a polymer binder in the formulation, therefore, it acts as a polymer-matrix composite and possesses a nonlinear performance. Thus, one goal is to analyze its complex behavior by implementing a multi-linear isotropic hardening plasticity model on the experimental stress-strain data. For this purpose, a plane stress state was considered, and no plasticity was assumed in the fibre direction. The simulated results were then compared with the experimental ones. Moreover, the nanoindentation method was utilized to explore the elastic and hardness properties of the ink at a small-scale and obtained results were compared with the theoretical values determined by the Oliver-Pharr method.

2.0 THEORETICAL BACKGROUND

2.1 Constitutive Law of Plasticity

The elastic-plastic analysis of polymeric composites takes part in the synthesis and evaluation of structural integrity of different components in various applications. The loading condition in the elastic-plastic analysis depends on the type of application and may vary accordingly from simple monotonic loading to cyclic loading. A plastic constitutive model must have the yield criterion function, which is used to define the state of a material from elastic to elastic-plastic behavior during the transition, plastic strain increment due to the load increment is determined by the flow rule, and the hardening rule used to evaluate the yield criterion during plastic deformation.

The plastic behavior of a material is described by implementing the flow plasticity theory, based on an assumption that the amount of plastic deformation in a material is determined by a flow rule. It is also considered that the total strain tensor increment of a material is obtained by adding the elastic and plastic strain tensors increments together, as shown in Eq. (1). However, the elastic strains are obtained through a linear elastic, whereas for strains in the plastic region are calculated by flow rule and different hardening models.

$$d\varepsilon^t = d\varepsilon^{el} + d\varepsilon^{pl} \tag{1}$$

Likewise, other constitutive models, the elastic-plastic models are based on the Helmholtz free energy function per unit volume (strain energy density function). This function depends on the structural tensor (A), elastic strain or total strain (ε^t), plastic strain (ε^{pl}) and the hardening coefficient (κ) [56]. The constitutive formulation of strain energy density function is expressed in Eq. (2) as:

$$W(\varepsilon^{el}, A, \kappa) = W(\varepsilon^{total}, \varepsilon^{pl}, A, \kappa,) = \frac{1}{2}\varepsilon^{el}{:}\,C^{el}{:}\,\varepsilon^{el} + W^{hard}(A, \kappa) \tag{2}$$

where, C^{el} or C_{ijkl} is the fourth-order elastic tensor and $W^{hard}(\kappa)$ represents the free-energy function with the hardening rule. Furthermore, the stress tensor (σ) is calculated on the basis of standard arguments [57] by taking the differential of the strain function in respect of the elastic strain tensor. Also, the elastic tensor (C^{el}) for transversely isotropic materials, is obtained by partial differentiating two times the strain function in respect of the elastic strain tensor as expressed in Eq. (3).

$$\sigma = \frac{dW}{d\varepsilon^{el}} = C^{el}{:}\,\varepsilon^{el} \tag{3}$$

2.2 Formation of Yield Function, Plastic Flow Rule and Hardening Rule

There are two yield criteria used in plasticity models: Von Mises and Hill yield criterion. The von Mises yield criterion is utilized for the plastic behavior of several materials like metals, polymers and their composites. This function is independent of the hydrostatic pressure and is considered an isotropic criterion. It is, therefore, not useful for the application of micro-structured materials that demonstrates plastic expansion. However, for materials such as forged metals and composites, the Hill yield criterion is used to develop the respective constitutive model in which the macroscopic behavior of the material is influenced by the microstructural behavior. It is an anisotropic criterion which is based on the direction of the stress with respect to the axis of anisotropy. Thus, a von Mises yield criterion is used in this study to analyze the nonlinear behavior of an isotropic and incompressible silver-based conductive ink.

According to the von Mises yield criterion, the yield function for homogenous, isotropic materials in the plastic regime can be expressed as:

$$F(\sigma_{ij}) = f(\sigma_{ij}) - \sigma_y = |\sigma_{eff}| - \sigma_y \tag{4}$$

where, σ_{ij} is the Cauchy stress tensor that has three principal or normal stresses (σ_1, σ_2 and σ_3), $F(\sigma_{ij})$ is the von Mises yield criterion function with the deviatoric components of normal stresses along i and j axis. $f(\sigma_{ij})$ and σ_y represent the von Mises effective stress ($\sigma_{eff} = \sigma_{eq}$ = equivalent stress) based on the stress tensor and corresponding yield stress in uniaxial loading, respectively. However, the main purpose of the yield function is to create a surface boundary between the elastic and plastic behavior of materials in the stress space which is known as the yield surface. The yield surface can be expressed in terms of principal stresses or invariants and is different for different plasticity models.

The direction or evolution of the plastic straining can be determined by calculating the plastic flow rule. The general formation of the plastic flow rule in terms of the plastic flow potential function of stresses comprised of different quantities and hardening parameters can be modelled as depicted in Eq. (5).

$$d\varepsilon^{pl} = d\lambda\frac{\partial Q}{\partial \sigma} \tag{5}$$

where, $d\lambda$ is the proportionality constant, termed as a plastic multiplier that can be obtained using different hardening rules and must be greater than 0. This multiplier helps in determining the amount of plastic straining. $Q = Q(\sigma)$ is the plastic flow potential function. However, there are two types of plastic flow rules: associated and non-associated flow rule. If the plastic flow potential function has the same value as that of the yield criterion function, i.e., $Q = F(\sigma)$, then the flow rule is known as the associative plastic flow rule. This condition is only valid for stable materials that possess convex yield surfaces, and their plastic strain increment vectors are acted normal to the yield surfaces. On the other hand, when the plastic flow potential function is not equal to the yield criterion function ($Q \neq F(\sigma)$), then the flow rule is said to be non-associated. The non-associated flow rule is used to describe the hardening behavior of unstable materials like soils and powdered materials. The plastic strain of these materials occurs due to the internal friction sliding behavior of the material. Also, the direction of plastic strain increment is not similar to that of the stress increment.

In consequence, the associative flow rule is opted for the formation of elastic-plastic model which works on the assumption of no plastic strain at $F(\sigma) < 0$ and $|\sigma_{eff}| < \sigma_y$. The material then behaves elastically, and the elastic stress range is defined by $|\sigma_{eff}| < \sigma_y$. The constitutive equation for stress increment becomes,

$$\frac{d\sigma}{dt} = C^{el}\left(\frac{d\varepsilon^t}{dt} - d\lambda\frac{\partial F(\sigma)}{\partial\sigma}\right) \tag{6}$$

The yield criterion of several materials is based on the loading and calculation of the plastic strain values. However, the loading can change the yield criterion which is known as hardening of the material. The hardening behavior of any material is defined by means of the hardening rule that explains the change in yield surface from one state to another via increment in the respective yield stress value in order to establish the stress states for successive yielding. The most commonly used hardening rules are isotropic and kinematic hardening rules.

The material is said to undergo isotropic hardening when the yield surface in a particular stress space remains unchanged and centred along its initial centreline where all principal stresses are the same ($\sigma_1 = \sigma_2 = \sigma_3$). Also, the size of the yield surface increases or decreases during the development of the plastic strains. It is also not applicable for cyclic loading because it does not consider the Bauschinger effect. On the other hand, in the kinematic hardening rule, the translation of the yield surface via stress space occurs along with the progressive yielding, but the size and shape of the yield surface remain unchanged. As a matter of fact, the kinematic hardening rule is applicable for modelling the nonlinear behavior of materials under cyclic loading. It is used to model different material behavior, such as Baushinger effects in which the compressive yield stress is less than the tensile yielding and ratcheting behavior which is helpful in building the plastic strains during repetitive loading.

2.3 Multi-linear Isotropic Hardening Plasticity Model

The multi-linear isotropic hardening model is one of the simplest elastic-plastic models used in uniaxial loading which generates the total stress-strain curve with positive stress-strain values. The von Mises yield criterion is used with the associative plastic flow rule and isotropic hardening rule in this model.

As per von Mises criterion, it is assumed that the stress state point occurs on the yield surface; therefore, the effective stress is considered to be the same as the yield stress. Because of this condition, the yield function will become zero and shows plastic deformation under continuous loading. However, the von Mises effective stress is expressed as:

$$\sigma_{eff} = \sqrt{\frac{(\sigma_1 - \sigma_2)^2 + (\sigma_2 - \sigma_3)^2 + (\sigma_3 - \sigma_1)^2}{2}} = \sqrt{\frac{3}{2}s_{ij}s_{ij}} \tag{7}$$

where, s_{ij} denotes as the elements of deviatoric stress tensor given in Eq. (8) as:

$$s_{ij} = \sigma - \frac{1}{3}tr(\sigma)^2 \tag{8}$$

In the principal stress space, the yield surface along the hydrostatic axis generates a von Mises yield criterion function, which is independent on the hydrostatic stress. Hence, the yield function for a multi-linear isotropic hardening model is represented in Eq. (9) as:

$$F(\sigma) = |\sigma_{eff}| - \sigma_y = \sqrt{\frac{3}{2}s_{ij}s_{ij}} - \sigma_y = 0 \tag{9}$$

The parameter σ_y denotes the final yield stress, which is based on the plastic work done. It can be calculated from the effective plastic strain and stress-strain curve data as expressed in Eq. (10).

$$\sigma_y = E^{pl}\varepsilon_{eff}^{pl} \tag{10}$$

$$\because \quad E^{pl} = \frac{E^{el}E^{ep}}{E^{el} - E^{ep}} \tag{11}$$

where, E^{pl} is the plasticity modulus, E^{el} denotes the modulus of elasticity and E^{ep} represents the elastic-plastic modulus or tangent modulus obtained from the engineering stress-strain data. However, the general formation of the loading surface with isotropic hardening is illustrated as:

$$F(\sigma, k) = f(\sigma) - k\left(\varepsilon_{eff}^{pl}\right) \tag{12}$$

The parameter $k(\varepsilon_p)$ represents the internal variable which is dependent on the effective plastic strain, not the strain path and shows the hardening of respective material. For the von Mises yield criterion, the hardening parameter (k) can be evaluated by using Eq. (13) as:

$$\frac{dk(\varepsilon_{eff}^{pl})}{dt} = h\frac{d\varepsilon_{eff}^{pl}}{dt} \rightarrow k(\varepsilon_{eff}^{pl}) = \sigma_{yo} + h\varepsilon_{eff}^{pl} \tag{13}$$

where h is the material constant and σ_{yo} represents the initial yield stress. In addition, a Ludwig equation (power curve relation) [58,59] is used to calculate the strain hardening index (n) and strength coefficient (K) also known as isotropic hardening modulus, by applying Eq. (14) on the simulated true stress-strain data as:

$$\sigma = \sigma_y + \mathrm{K}\varepsilon^n \tag{14}$$

3.0 EXPERIMENTAL AND NUMERICAL ANALYSIS

This section focused on the fabrication and evaluation of the mechanical properties of conductive ink using tensile testing and nanoindentation technique. The material characterization was also carried out using a multi-linear isotropic hardening rule plasticity model. Results obtained from the tensile test were used to calibrate and validate using FEM.

3.1 Materials

Poly(dimethylsiloxane) hydroxy-terminated (PDMS-OH) of 110 × 10^3 g/mol molecular weight and 50 × 10^3 cSt viscosity used as a binder or epoxy resin. (3-glycidyloxypropyl) trimethoxysilane (ETMS) with 236.34 g/mol molecular weight, ≥98% purity, and 1.07 g/ml specific gravity at 25°C worked as a cross-linking agent that connects the binder with conductive filler. Octamethylcyclotetrasiloxane (D4) served as an organic solvent which is 99% pure with a molecular weight of 92.14 g/mol. Silver flakes of 2-3.5 µm size were used as a conductive filler, whereas the viscosity of the mixture was controlled by 99% pure toluene (92.14 g/mol molecular weight). Two catalysts were used to speed up the reaction: acetic acid (99% pure) and dibutyltin dilaurate (DBDTL – 631.56 g/mol molecular weight, 95% purity). All these chemicals were purchased from Sigma Aldrich.

3.2 Fabrication of Conductive Ink

The silver-based conductive ink was fabricated by mixing silver flakes with the base polymer PDMS-OH. Toluene was added and mixed in the solution for 24 hours on a magnetic stirrer at 220-280 rpm to dissolve all the silver particles in the binder. When all the silver particles were dissolved, then some amount of D4 and ETMS were added and mixed for further 5-10 minutes depending upon the solubility of the mixture. Lastly, some drops of acetic acid and DBDTL were added to the mixture before curing. The conductive ink mixture was then dispensed on a rectangular-shaped mould of specifications shown in Figure 1(a), and curing was done for 24 hours at room temperature. Three samples were made using the same procedure and proceeded to the experimentation.

3.3 Uniaxial tensile testing

The mechanical properties of formulated silver-based conductive ink were investigated initially by uniaxial tensile testing on UTM Instron 3360 at room temperature in the Rubber lab of USM. The test was carried out on three samples of ink at a loading rate of 10 mm/minute and 10 kN load cell. The schematic illustration of ASTM D412 type C standard dog-bone-shaped geometry and the ink sample with the rectangular portion of the standard is shown in Figure 1.

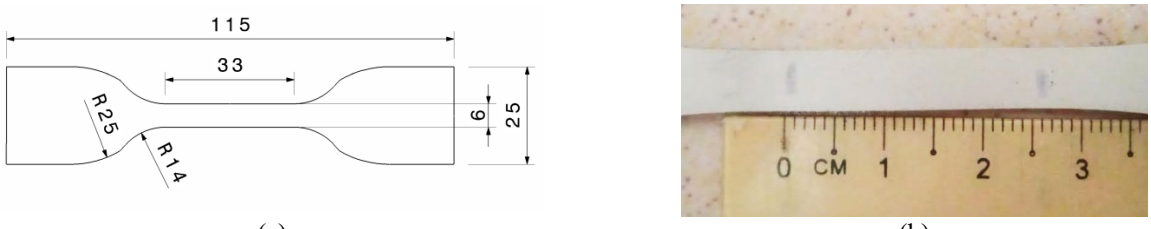

(a) (b)

Figure 1. (a) Dog-bone shaped standard geometry, (b) the rectangular silver ink sample

To perform the experiment, the silver ink sample was fixed between the jaws at the length of 25 mm, which is the actual gauge length of the dog-bone standard. Three samples were tested one at a time. The stress-strain data of every sample was generated, and the final curve of the ink was plotted between the average engineering stress and engineering strain values of all three samples, as illustrated in Figure 2. This data was then utilized in a multi-linear isotropic hardening model, and FE analysis was done as explained in the following section.

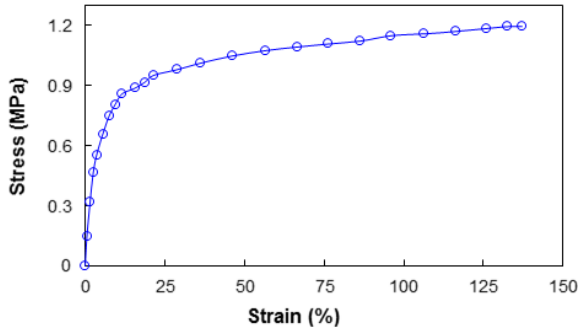

Figure 2. Graphical representation of stress-strain data of silver-based conductive ink from UTM. The x-axis denotes the engineering strain and y-axis represents the engineering stress data

3.4 Calculation of Material Properties by Plasticity Model

The material characterization of formulated silver-based conductive ink was done by applying the experimental data on the multi-linear isotropic hardening plasticity model in Abaqus. The purpose of curve fitting analysis was to determine the approximated stress-strain curve that fit closely to the engineering stress-strain data. For curve fitting, Young's modulus, yield stress, and plastic strain data were required. In order to get the yield stress and plastic strain values, the engineering stress-strain values from tensile testing were converted to the true stress and true strain, respectively, using Eq. (15) and (16). The true stress was represented as the yield stress, while the plastic strain values were obtained by subtracting the elastic true strain from the total true strain as expressed in Eq. (17). Lastly, the calculated yield stress and plastic strain data were used for further analysis.

$$\varepsilon^{true} = \ln(1 + \varepsilon^{eng}) \tag{15}$$

$$\sigma^{true} = \sigma^{eng} e^{\varepsilon^{true}} = \sigma^{eng}(1 + \varepsilon^{eng}) \tag{16}$$

$$\varepsilon^{pl} = \varepsilon_t^{true} - \frac{\sigma^{true}}{E^{el}} \tag{17}$$

where ε^{true} represents the true strain, σ^{true} is the true stress, ε^{eng} denotes the engineering strain and σ^{eng} is the engineering stress. ε^{pl} gives the true plastic strain value, while the total true strain is symbolized as ε_t^{true}.

3.5 Nanoindentation Method

The main principle of nanoindentation is to allow the indenter to penetrate the material by employing a high-resolution force actuator. Due to this penetration, the elastic and plastic deformations occur, and the hardness value of a material is then calculated. After removing the indenter from the material, the part that is covered is only the elastic part of the displacement, and from this, one can calculate the modulus of elasticity of the material. However, in this study, the nanoindentation technique was utilized to examine the mechanical properties of formulated silver-based conductive ink at the micro or nano level. The test was conducted on the Micro Materials NanoTest Vantage machine with a three-sided pyramidal indenter named Berkovich. This type of indenter has been widely used in the testing of various materials because it helps to induce the plasticity at very small loads and measure the hardness. The Berkovich indenter also reduces the influence of friction due to its large included angle. The synopsis of the platform of NanoTest Vantage machine in the Nanofabrication & Functional Material lab of USM is depicted in Figure 3.

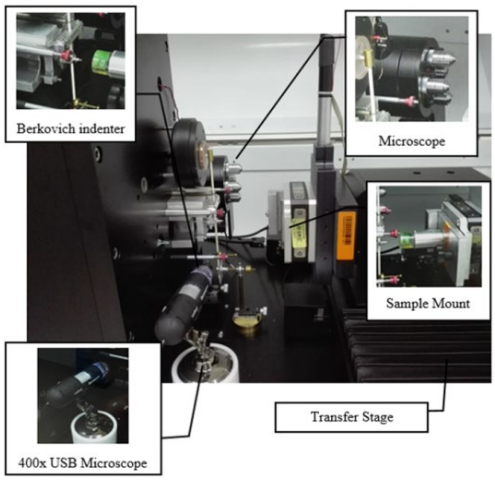

Figure 3. Platform of NanoTest Vantage machine.

A small amount of conductive ink sample with a thickness of 3 mm was mounted on the stub by applying cyanoacrylate adhesive between the interface of the sample and the stub. The stub was screwed onto the sample plate and placed into the working station on the machine by sliding the sample plate down. The sample plate was tightened on the sample mount until both became parallel to each other. For the new experiment and indent position definition, the transfer stage was moved back to the microscope position. The area of indentation on the sample was recognized by the visible light and scanning probe microscopes. The new recalibrate nanoindentation experiment was defined to ensure high precision in the nanoindentation experiment. The default parameters were used except the loading rate, dwell time and maximum load. Based on the literature, for soft materials like rubbers or rubber-like materials, various maximum loads have been used in accordance with the dwell time and loading rate [60–63]. In this analysis, a 5 mN load was applied to the material with a loading and unloading rate of 0.5 mN/s and dwell time of 2 secs. Ten indentations were marked on two specimens under both loads, and their respective average load-displacement curves were calculated. The obtained hardness and reduced modulus values were also validated by Oliver and Pharr's method [64].

The typical load-displacement curve that gives the values of maximum load (P_{max}), maximum displacement (h_{max}) and elastic unloading stiffness or contact stiffness (S) (slope of unloading curve) can be found in [40]. As per the curve, the unloading curve behaves non-linearly, so, the power-law can be used to interpret the unpredictable behavior of the material in which the values of load (P) and depth (h) can be taken at any point of the curve [65] as:

$$P = \alpha(h - h_f)^m \tag{18}$$

where, m is the geometry constant of the indenter, which is equal to 1.5 for the Berkovich indenter, while α is the material constant which can be found from the regression analysis. Theoretically, the final depth after complete unloading is denoted by h_f but in the Oliver-Pharr method, it represents the fitting parameter obtained via the regression method. For fitting the power law, only the upper unloading data is used.

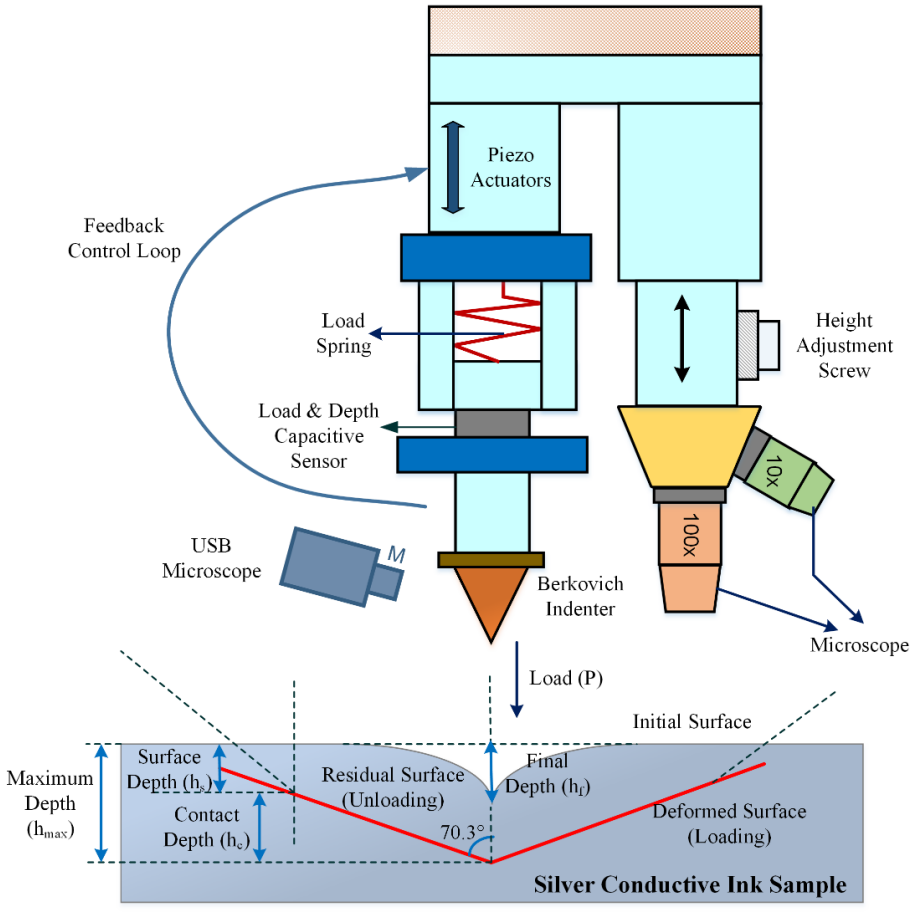

Figure 4. Loading and unloading process showing parameters during nanoindentation

The schematic representation of nanoindentation machine alongwith loading, unloading, and sink-in of the material during nanoindentation is shown in Figure 4. It is important to assume that the contact periphery sinks in a manner which can be described by models for indentation of a flat elastic half-space by rigid punches of simple geometry. Assuming that pile-up is negligible, the elastic model shows the amount of sink-in, h_s is given in Eq. (19), where ϵ (geometry constant of indenter) = 0.75 for paraboloid Berkovich indenter with an angle of $\phi = 70.3°$. The contact depth (h_c) is used to calculate the projected contact area, i.e., $A = F(h_c)$ as shown in Eq. (20). However, from Fischer-Cripp [66], the projected area of the contact is obtained by Eq. (21).

$$h_s = \epsilon \frac{P_{max}}{S} \tag{19}$$

$$h_c = h_{max} - \epsilon \frac{P_{max}}{S} \tag{20}$$

$$A_p = 24.49 {h_c}^2 \tag{21}$$

After calculating the projected area, the hardness, elastic modulus and stiffness can be calculated using Eq. (22), (23) and (24), respectively.

$$H = \frac{P_{max}}{A} \tag{22}$$

$$\frac{1}{E_r} = \frac{1 - {\nu_s}^2}{E_s} + \frac{1 - {\nu_i}^2}{E_i} \tag{23}$$

$$S = \frac{dP}{dh} = \beta \frac{2}{\sqrt{\pi}} E_r \sqrt{A} \tag{24}$$

where, β represents the geometry shape factor of Berkovich indenter and is equal to 1.034. Based on the value of geometry shape factor, plastic depth (hp) is the same as the contact depth (h_c) when $\beta = 1$ or near to 1. For the present study, it was assumed that $h_p = h_c$ and the modulus of elasticity (E_i) and Poisson's ratio of indenter were taken as 1141 GPa and 0.07, respectively. From Figure 5, it can be seen that the unloading curve behaves non-linearly; therefore, Eq. (18) can be used to define the nonlinear behavior of the material in which the values of load (P) and depth (h) are taken at any instant of the curve [65]. The reduced modulus (E_r) was obtained from the nanoindentation test and Poisson's ratio for silver-based conductive ink was considered as 0.37. These values were then compared with the tensile testing Young's modulus.

4.0 RESULTS AND DISCUSSIONS

The experimental test data obtained from the uniaxial tensile testing machine was implemented on the multi-linear isotropic hardening plasticity model in simulation software. The curve-fitting results were then compared with the experimental data in order to validate the results. Furthermore, the load-depth curve from nanoindentation and different parameters used in this technique were evaluated. The comparison between the elastic modulus obtained from tensile test and indentation was also done.

4.1 Application of plasticity model and simulation results

Since conductive ink is a combination of rubber-like material and conductive filler, therefore, it is considered as a polymeric composite that has both elastic and plastic properties. Such type of composites possesses nonlinear behavior under tensile loading due to the presence of base polymer and do not obey simple Hooke's law. Subsequently, to study the complex behavior of polymeric composites, the constitutive modeling in respect of the elastic, perfectly-plastic or elastic-plastic nature of the material is carried out. In the present study, the experimental stress-strain data of silver-based conductive ink were converted to equivalent plastic strain and yield stress data using mathematical expressions of true strain and true stress, respectively. This data was then imported to the simulation software, and FE analysis was done.

A 3D rectangular-shaped model of the ink, having a geometry similar to that used for tensile testing, was generated into a commercially available FE software Abaqus. The elastic properties of the ink were taken as 5.72 MPa Young's modulus and Poisson's ratio 0.37. Similarly, for elastic-plastic analysis, the calculated plastic strain and yield stress data from tensile testing were added to the plasticity section of the material properties and isotropic hardening was chosen. The hexahedral elements with linear formulation C3D8RH were opted for meshing. This type of meshing represents the 8-node linear bricks, hybrid formulation, constant pressure and reduced integration along with the hourglass control. The boundary conditions were applied at both ends of the sample after meshing. One end was fixed in all directions, i.e., $U_x = U_y = U_z = 0$, while on the other end, 25 mm displacement in the y-direction was implemented, and the displacement along two directions, x and z, were equal to 0, i.e., $U_x = U_z = 0$. The applied boundary conditions and meshing of the proposed parametrized FE model for silver-based conductive ink are described in Figure 5.

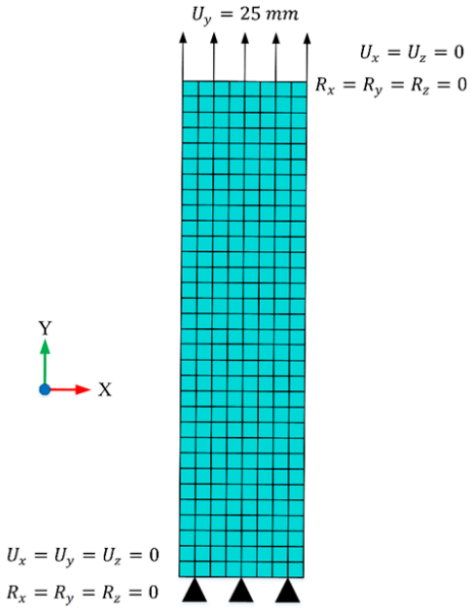

Figure 5. FE model of silver ink with meshing and boundary conditions

The simulations were accomplished on a machine with 3.60 GHz Intel(R) Xenon Core 4 CPU, 4 GB RAM and x64-based processors. The simulated and experimental true stress vs true total strain were expressed in Figure 6. It is worth noticing that the simulated results are in good agreement with the experimental data; therefore, the multi-linear isotropic hardening model is suitable for the current formulated ink under the aforementioned elastic properties.

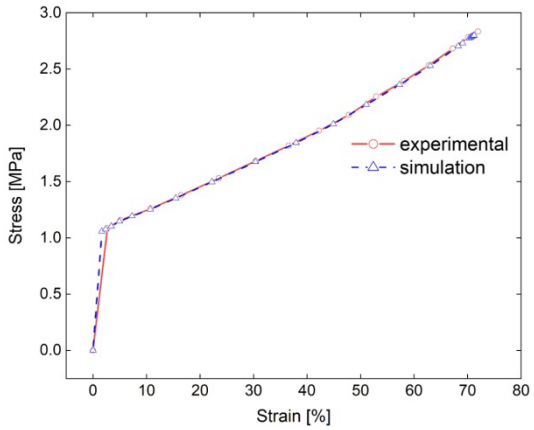

Figure 6. Comparison of true stress-strain data obtained experimentally and simulating the multi-linear isotropic hardening model. The x-axis denotes true strain, and y-axis represents true stress

Furthermore, the true stress-strain curve for the elastic-plastic model is comprised of elastic and plastic regimes; therefore, the strain hardening and hardening modulus of the material also plays a vital role in studying the plastic behavior. As a matter of fact, the strain hardening index or work hardening parameter (n) is defined as the measurement of a material to gain strength quickly under deformation. Thus, for the isotropic hardening plasticity model, the power law was used to fit the simulated true stress-strain data in order to evaluate the strain hardening exponent (n) and isotropic hardening modulus (K). The values of these material constants after curve fitting were obtained as 1.268 and 2.625 MPa, respectively, with the coefficient of determination (R^2) equal to 0.9994.

4.2 Nanoindentation Experiment

The nanomechanical properties such as elastic modulus, hardness, plastic deformation, and elastic and plastic work, of silver-based conductive ink were investigated by the nanoindentation technique. A load-controlled mechanism was used to make ten indents on the sample at equal lengths. The material started to deform soon after the application of the indenter on the surface of the sample. The peak load applied to the sample was 5 mN with 2 secs dwell or holding time and 0.5 mN/s loading and unloading rate. The loading and unloading curve obtained after every indent giving the respective load and depth data points. The average of these data points was taken to analyze the behavior of formulated ink at the nanoscale level. Figure 7 shows the load-depth curve of the ink.

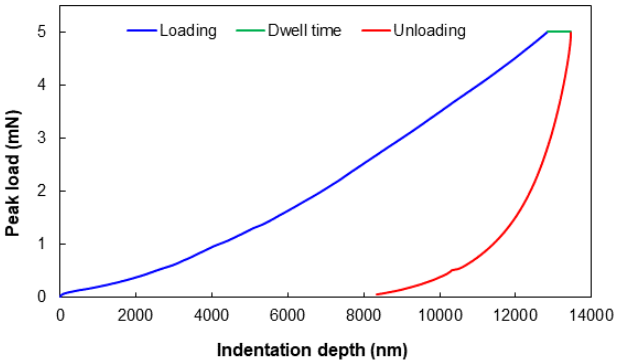

Figure 7. Load (P) and depth (h) curve of conductive ink.

It can be seen from the above figure that the plastic work of the sample is represented by the area under the curve and the area from maximum depth (h_{max}) to the permanent deformation or the final depth (h_f) denotes the elastic work. This graph shows that the ink exhibited both elastic-plastic behavior depending on the applied load, loading/unloading rate and holding time. Furthermore, the Oliver-Pharr method was used to calculate the reduced modulus, modulus of elasticity, stiffness and hardness values of the sample theoretically and then compared with the indentation test results as illustrated in Table 1.

Table 1. Mechanical properties of silver-based ink by nanoindentation technique

Parameters	Nanoindentation machine	Oliver-Pharr method	% error
Reduced modulus (E_r)	34.53 MPa	38.04 Mpa	9.23
Stiffness (dP/dh)	0.000105 mN/nm	0.0001048 mN/nm	0.19
Modulus of elasticity (E_s)	29.80 MPa	32.83 MPa	9.23
Hardness (H)	1.45 MPa	1.424 MPa	1.83

From Table 1, it can be inferred that the elastic modulus, reduced modulus, and hardness of silver-based conductive ink obtained by nanoindentation and the Oliver-Pharr method are somehow in good agreement with each other. In addition, the reduced modulus can be calculated through nanoindentation, which depends on the stiffness or slope of the unloading curve. The stiffness is measured at the start of the unloading curve, and because of this reason, the reduced modulus values become very high, whereas such values may decrease in the lower part of the unloading curve. Despite this, the elastic modulus obtained by nanoindentation (29.80 MPa) was compared with that of the tensile measurements (5.72 MPa) and found that it was very high as compared to the tensile modulus of elasticity. This is because the evaluation of the modulus of elasticity of polymers and their composites mainly depends on the type and environment of the experimentation used for the analysis. Based on the soft nature and variation in the properties of these materials under different working environments, the elastic modulus values from the uniaxial tensile test and nanoindentation technique are not similar to each other. Thus, the elastic modulus is always higher during indentation method than the tensile testing because of the following reasons: (a) the polymers are not homogenous throughout the length scales; (b) the indentation measurements are limited to the region of indenter contact, that is from millimetres to nanometers, depending on the indenter size and geometry; (c) the macroscopic deformations occur during tensile measurements using the full-length sample; and (d) the elastic modulus from indentation is perpendicular to the orientation of the sample, whereas, the tensile test provides the modulus along the direction of the sample.

Consequently, the present study examined the mechanical and material characterization of silver-based conductive ink under macro and micro levels of testing and constitutive modelling. Several formulations for conductive inks have been proposed by various scientists to evaluate their modulus of elasticity, stretchability and hardness values depending on the application. However, the obtained results of this research are compared with the associated work, as illustrated in Table 2. According to Table 2, it can be observed that the current formulation of silver-based conductive ink at room temperature exhibited good stretchability with respective modulus of elasticity than the other conductive inks, as these inks mostly required higher temperatures of fabrication and curing. However, the key factors in designing a good conductive ink are the manufacturing process, fabrication and curing temperatures, conductive filler and the polymer binder. So, by considering all the factors, it can be said that Ag-PDMS conductive ink is useful for stretchable electronic devices with up to 137% stretchability and 1.45 MPa hardness.

Table 2. Comparison of current research findings with the other related studies

Ref.	Conductive Material		Polymer matrix	Stretchability	Elastic modulus	Hardness
	Filler	Size				
[67]	CuNWs	10 wt.%	PHB	-	-	0.35 GPa
		10 wt.%	PHO	-	-	0.0137GPa
[68]	MWCNTs	0.75 wt.%	Epoxy-acrylate	-	2.05 GPa	0.094 GPa
[69]	Ag flakes	0.6-4.0 µm (70%)	Acrylic polymers	-	492±39 Pa	-
[70]	CuNWs	L = 20 µm D = 60 nm	PVA-PDMS	60%	37.5 kPa	-
[71]	Ag powder	2-3.5 µm	PDMS	150%	8 MPa	-
[72]	AgNWs	L = 8 µm D = 60 nm	PLA	3%	3048 MPa	-
[73]	CNT	0.5 wt.%	TPU	-	74.8 MPa	83.6 MPa
	Modified CNT	0.5 wt.%			65 MPa	84.5 MPa
[74]	AgNPs	> 100 nm	PVP	130%	-	-
[75]	AgNPs	< 100 nm	PDMS	70%	-	-
Present study	Ag powder	2-3.5 µm	PDMS-OH	137%	5.72 MPa	1.45 MPa

Note: CuNWs: Copper nanowires, MWCNTs: Multi-walled carbon nanotubes, AgNWs: Silver nanowires, AgNPs: Silver nanoparticles, PHB: Polyhydroxybutyrate, PHO: Polyhydroxyoctanoate, PVA: Polyvinyl alcohol, PDMS: Polydimethylsiloxane, PLA: Polylactide, TPU: Thermoplastic polyurethane, PVP: Polyvinylpyrrolidone

5.0 CONCLUSIONS

The purpose of this study is to investigate the mechanical properties of formulated silver-based conductive ink for stretchable electronics applications. Two methods opted for experimental analysis: uniaxial tensile testing and nanoindentation technique. Initially, the ink was fabricated using silver powder as a conductive filler and PDMS-OH as a binder. The following results were obtained during this study:

i. The modulus of elasticity, tensile strength and yield stress of the ink at 137% stretchability before rupture were obtained as 5.72 MPa, 1.195 MPa and 0.86 MPa, respectively.
ii. The experimental stress-strain data, in the form of yield stress and plastic strain values, was implemented on the multi-linear isotropic hardening plasticity model to analyze the complex behavior of the ink.
iii. As a consequence, the simulation results were in good agreement with the experimental true stress-strain values. However, these results may be slightly changed from the experimental because of the change in thickness and displacement values.
iv. In addition, the nanoindentation technique was utilized to determine the hardness and elastic modulus values of the silver conductive ink at 5 mN peak load, 0.5 mN/s loading rate and 2 sec holding time as 1.45 MPa and 29.80 MPa, respectively.
v. The nanoindentation results were compared with the theoretical values obtained by the Oliver-Pharr method, and as a result, it is concluded that the nanoindentation method is designed on the theory proposed by Oliver and Pharr.
vi. Moreover, the modulus values obtained from nanoindentation are very high than the elastic modulus of tensile testing because the indentation measurements are limited to the region of indenter contact, while, in tensile testing, the modulus is measured using the full-length sample.
vii. Lastly, the mechanical properties of the proposed silver-based conductive ink were compared with the other formulations proposed by many researchers, and it was found that the current silver ink could stretch up to 137% with 1.45 MPa hardness for particular applications such as wearable electronics.

6.0 ACKNOWLEDGEMENT

The authors would like to thank University Sains Malaysia (USM) for funding this project under Research University Grant 1001.PMEKANIK.8014067 and Short-Term Grant 304.PMEKANIK.6315494.

7.0 REFERENCES

[1] Y. Su, C. Ma, J. Chen, H. Wu, W. Luo, et al., "Printable, highly sensitive flexible temperature sensors for human body temperature monitoring: A review," *Nanoscale Research Letters*, vol. 15, p. 200, 2020.
[2] F. Akther, S.B. Yakob, NT. Nguyen, and H.T. Ta, "Surface modification techniques for endothelial cell seeding in PDMS microfluidic devices," *Biosensors*, vol. 10, pp. 1-18, 2020.
[3] J. Casanova-Moreno, J. To, C.W.T. Yang, R.F.B. Turner, D. Bizzotto, and K.C. Cheung, "Fabricating devices with improved adhesion between PDMS and gold-patterned glass," *Sensors & Actuators, B: Chemical*, vol. 246, pp. 904–909, 2017.
[4] S. Zulfiqar, A.A. Saad, M.W. Chek, M.F.M. Sharif, Z. Samsudin, and M.Y.T. Ali, "Structural and random vibration analysis of LEDs conductive polymer interconnections," *IOP Conference Series: Materials Science and Engineering,* vol. 815, pp.1-15, 2020.

[5] S. Zulfiqar, A.A. Saad, M.F.M. Sharif, Z. Samsudin, M.Y.T. Ali, et al., "Alternative manufacturing process of 3-dimensional interconnect device using thermoforming process," *Microelectronics Reliability,* vol. 127, p. 114373, 2021.

[6] L. Hu, J. Choi, S. Hwangbo, D-H. Kwon, B. Jang, et al., "Flexible micro-LED display and its application in Gbps multi-channel visible light communication," *NPJ Flexible Electronics*, vol. 6, p. 100, 2022.

[7] L. Hu, and J-H. Ahn, "Flexible and stretchable micro-LED display," in *Micro light emitting diode: Fabrication and devices. series in display science and technology,* Ahn J-H, Kim J-H, Eds. Singapore: Springer, 2021, pp. 141–160.

[8] X-F. Zhao, S-Q. Yang, X-H. Wen, Q-W. Huang, P-F. Qiu, et al., "A fully flexible intelligent thermal touch panel based on intrinsically plastic Ag2S semiconductor," *Advanced Materials*, vol. 34, p. 2107479, 2022.

[9] C. Wang, X. Li, H. Hu, L. Zhang, Z. Huang, et al., "Monitoring of the central blood pressure waveform via a conformal ultrasonic device," *Nature Biomedical Engineering*, vol. 2, pp. 687–695, 2018.

[10] Y. Liu, J-R. Riba, M. Moreno-Eguilaz, and J. Sanllehí, "Analysis of a smart sensor based solution for smart grids real-time dynamic thermal line rating," *Sensors*, vol. 21, p. 7388, 2021.

[11] S. Wang, J. Xu, W. Wang, G.J.N. Wang, R. Rastak, et al., "Skin electronics from scalable fabrication of an intrinsically stretchable transistor array," *Nature,* vol. 555, pp. 83–88, 2018.

[12] S. Chen, L. Sun, X. Zhou, Y. Guo, J. Song, et al., "Mechanically and biologically skin-like elastomers for bio-integrated electronics," *Nature Communications,* vol. 11, p. 1107, 2020.

[13] H-L. Cao, and S-Q. Cai, "Recent advances in electronic skins: material progress and applications," *Frontiers in Bioengineering and Biotechnology,* vol. 10, pp. 1-8, 2022.

[14] S. Zulfiqar, A.A. Saad, Z. Ahmad, F. Yusof, and Z. Bachok, "Structural analysis and material characterization of silver conductive ink for stretchable electronics," *International Journal of Integrated Engineering,* vol. 13, pp. 128–35, 2021.

[15] S. Park, M. Vosguerichian, and Z. Bao, "A review of fabrication and applications of carbon nanotube film-based flexible electronics," *Nanoscale*, vol. 5, pp. 1727–1752, 2013.

[16] Y. Zhang, S. Wang, X. Li, J.A. Fan, S. Xu, et al., "Experimental and theoretical studies of serpentine microstructures bonded to prestrained elastomers for stretchable electronics," *Advanced Functional Materials,* vol. 24, pp. 2028–2037, 2014.

[17] D. McCoul, W. Hu, M. Gao, V. Mehta, and Q. Pei, "Recent advances in stretchable and transparent electronic materials," *Advanced Electronic Materials*,vol. 2, p. 1500407, 2016.

[18] J.A. Rogers, T. Someya, Y. Huang, "Materials and mechanics for stretchable electronics," *Science*, vol. 327, pp. 1603–1607, 2010.

[19] D.S. Saidina, N. Eawwiboonthanakit, M. Mariatti, S. Fontana, and C. Hérold, "Recent development of graphene-based ink and other conductive material-based inks for flexible electronics," *Journal of Electronic Materials,* vol. 48, pp. 3428–3450, 2019.

[20] S. Samimi Gharaie, A. Seyfoori, B. Khun Jush, X. Zhou, E. Pagan, et al., "Silicate-based electro-conductive inks for printing soft electronics and tissue engineering," *Gels*, vol. 7, p. 240, 2021.

[21] A.S. Sergeev, A.R. Tameev, V.I. Zolotarevskii, and A.V. Vannikov, "Electrically conductive inks based on polymer composition for inkjet printing," *Inorganic Materials Applied Research*, vol. 9, pp. 147-150, 2018.

[22] T.Q. Trung, and N-E. Lee, "Recent progress on stretchable electronic devices with intrinsically stretchable components," *Advanced Materials*, vol. 29, pp. 1603167, 2017.

[23] A. Kamyshny, and S. Magdassi, "Conductive nanomaterials for printed electronics," *Small*, vol. 10, pp. 3515–3535, 2014.

[24] K. Gilleo, "Assembly with conductive adhesives," *Soldering & Surface Mount Technology*, vol. 7, no. 1, pp. 12-17, 1995.

[25] H. Li, K.S. Moon, and C.P. Wong, "A novel approach to stabilize contact resistance of electrically conductive adhesives on lead-free alloy surfaces," *Journal of Electronic Materials*, vol. 33, pp. 106-113, 2004.

[26] A.T. Ten Cate, C.H. Gaspar, H.L.K. Virtanen, R.S.A. Stevens, R.B.J. Koldeweij, et al., "Printed electronic switch on flexible substrates using printed microcapsules," *Journal of Materials Science,* vol. 49, pp. 5831-5837, 2014.

[27] J. Zhang, X. Li, X. Shi, M. Hua, X. Zhou, and X. Wang, "Synthesis of core-shell acrylic-polyurethane hybrid latex as binder of aqueous pigment inks for digital inkjet printing," *Progress in Natural Science: Materials International,* vol. 22, pp. 71–78, 2012.

[28] M. Amjadi, Y.J. Yoon, and I. Park, "Ultra-stretchable and skin-mountable strain sensors using carbon nanotubes-Ecoflex nanocomposites," *Nanotechnology,* vol. 26, pp. 375501, 2015.

[29] H. Talebi, M. Silani, SPA. Bordas, P. Kerfriden, and T. Rabczuk, "A computational library for multiscale modeling of material failure," *Computational Mechanics,* vol. 53, pp. 1047–1071, 2014.

[30] N. Vu-Bac, MA. Bessa, T. Rabczuk, and WK. Liu, "A multiscale model for the quasi-static thermo-plastic behavior of highly cross-linked glassy polymers," *Macromolecules*, vol. 48, pp. 6713–6723, 2015.

[31] N. Vu-Bac, P.M.A. Areias, and T. Rabczuk, "A multiscale multisurface constitutive model for the thermo-plastic behavior of polyethylene," *Polymer (Guildf),* vol. 105, pp. 327–338, 2016.

[32] M.A. Msekh, N.H. Cuong, G. Zi, P. Areias, X. Zhuang, and T. Rabczuk, "Fracture properties prediction of clay/epoxy nanocomposites with interphase zones using a phase field model," *Engineering Fracture Mechanics,* vol. 188, pp. 287–299, 2018.

[33] H. Lippmann, and J. Lemaitre, *A course on damage mechanics*. Heidelberg: Springer Berlin, 2012.

[34] E.N. Brown, R.B. Willms, G.T. Gray, P.J. Rae, C.M. Cady, et al., "Influence of molecular conformation on the constitutive response of polyethylene: A comparison of HDPE, UHMWPE, and PEX," *Experimental Mechanics,* vol. 47, pp. 381–393, 2007.

[35] D. Garcia-Gonzalez, R. Zaera, and A. Arias, "A hyperelastic-thermoviscoplastic constitutive model for semi-crystalline polymers: Application to PEEK under dynamic loading conditions," *International Journal of Plasticity,* vol. 88, pp. 27–52, 2017.

[36] K. Hachour, F. Zaïri, M. Naït-Abdelaziz, J.M. Gloaguen, M. Aberkane, and J.M. Lefebvre, "Experiments and modeling of high-crystalline polyethylene yielding under different stress states," *International Journal of Plasticity,* vol. 54, pp. 1–18, 2014.

[37] C. G'sell, and A. Dahoun, "Evolution of microstructure in semi-crystalline polymers under large plastic deformation," *Materials Science and Engineering: A,* vol. 175, pp. 183–199, 1994.

[38] C. Jin, and D.M. Ebenstein, "Nanoindentation of compliant materials using Berkovich tips and flat tips," *Journal of Materials Research*, vol. 32, pp. 435–450, 2017.

[39] T. Pertin T, G. Minatchy, M. Adoue, A. Flory, and L. Romana, "Investigation of nanoindentation as a fast characterization tool for polymer degradation study," *Polymer Testing,* vol. 81, pp. 06194, 2020.

[40] W.C. Oliver, and G.M. Pharr, "An improved technique for determining hardness and elastic modulus using load and displacement sensing indentation experiments," *Journal of Materials Research,* vol. 7, pp. 1564–1583, 1992.

[41] J. Zhou, Q. Cai, and F. Xu, "Nanoscale mechanical properties and indentation recovery of PI@GO composites measured using AFM," *Polymers (Basel),* vol. 10, pp. 1020, 2018.

[42] S. Ji, J. Yang, J. Zhao, Y. Hu, and H. Gao, "Study about mechanical property and machinability of polyimide," *Polymers (Basel)* vol. 10, pp.1-10, 2018.

[43] R. Ferencz, J. Sanchez, B. Blümich, and W. Herrmann, "AFM nanoindentation to determine Young's modulus for different EPDM elastomers," *Polymer Testing,* vol. 31, pp. 425–432, 2012.

[44] P.G. Allison, R.D. Moser, J.P. Schirer, R.L. Martens, J.B. Jordon, and M.Q. Chandler, "In-situ nanomechanical studies of deformation and damage mechanisms in nanocomposites monitored using scanning electron microscopy," *Materials Letters,* vol. 131, pp. 313–316, 2014.

[45] M.M. Shokrieh, M.R. Hosseinkhani, M.R. Naimi-Jamal, and H. Tourani, "Nanoindentation and nanoscratch investigations on graphene-based nanocomposites," *Polymer Testing,* vol. 32, pp. 45–51, 2013.

[46] J. Cha, G.H. Jun, J.K. Park, J.C. Kim, H.J. Ryu, and S.H. Hong, "Improvement of modulus, strength and fracture toughness of CNT/Epoxy nanocomposites through the functionalization of carbon nanotubes," *Composites Part B: Engineering,* vol. 129, pp. 169–179, 2017.

[47] R. Ansari, and M.K. Hassanzadeh Aghdam, "Micromechanics-based viscoelastic analysis of carbon nanotube-reinforced composites subjected to uniaxial and biaxial loading," *Composites Part B: Engineering,* vol. 90, pp. 512–522, 2016.

[48] G. Arora, and H. Pathak, "Modeling of transversely isotropic properties of CNT-polymer composites using meso-scale FEM approach," *Composites Part B: Engineering,* vol. 166, pp. 588–597, 2019.

[49] G. Arora, and H. Pathak, "Experimental and numerical approach to study mechanical and fracture properties of high-density polyethylene carbon nanotubes composite," *Materials Today Communications,* vol. 22, pp. 100829, 2020.

[50] H. Lee, S. Mall, P. He, D. Shi, S. Narasimhadevara, Y-H. Yun, et al., "Characterization of carbon nanotube/nanofiber-reinforced polymer composites using an instrumented indentation technique," *Composites Part B: Engineering,* vol. 38, pp. 58–65, 2007.

[51] A-Y. Jee, and M. Lee, "Comparative analysis on the nanoindentation of polymers using atomic force microscopy," *Polymer Testing*, vol. 29, pp. 95–99, 2010.

[52] Am. Díez-Pascual, M.A. Gómez-Fatou, F. Ania, and A. Flores, "Nanoindentation in polymer nanocomposites," *Progress in Materials Science,* vol. 67, pp. 1–94, 2015.

[53] X. Zhang, Y. Zheng, G-Y. Li, Y-L. Liu, and Y. Cao, "Indentation creep tests to assess the viscoelastic properties of soft materials: Theory, method and experiment," *International Journal of Nonlinear Mechanics,* vol. 109, pp. 204–212, 2019.

[54] M.S. Goodarzi, H. Hosseini-Toudeshky, and H. Ghashochi-bargh, "Nanoindentation characterization of glass/epoxy composite for viscoelastic damage interlaminar modeling," *Engineering Fracture Mechanics,* vol. 226, pp. 106873, 2020.

[55] Y. Wang, L. Shang, P. Zhang, X. Yan, K. Zhang, S. Dou, et al., "Measurement of viscoelastic properties for polymers by nanoindentation," *Polymer Testing,* vol. 83, p. 106353, 2020.

[56] A. Dean, N. Safdar, R. Rolfes, "A co-rotational based anisotropic elasto-plastic model for geometrically nonlinear analysis of fibre reinforced polymer composites: Formulation and finite element implementation," *Materials* (Basel, Switzerland) vol. 12, pp.1-18, 2019.

[57] J. Bonet, and R.D. Wood, *Nonlinear continuum mechanics for finite element analysis, 2nd edition*. Cambridge: Cambridge University Press; 2008.

[58] B.K. Choudhary, E. Isaac Samuel, K. Bhanu Sankara Rao, and S.L. Mannan, "Tensile stress-strain and work hardening behaviour of 316LN austenitic stainless steel," *Materials Science and Technology,* vol. 17, pp. 223–231, 2001.

[59] Uijl N.J. Den, and L.J. Carless, "Advanced metal-forming technologies for automotive applications," in: *Advances in Materials Science and Engineering*, J. Rowe, Ed., United Kingdom: Elsevier, 2012, pp. 28–56.

[60] S. Yasin, A. Shakeel, T. Iqbal, F. Ahmad, H. Mehmood, et al., "Effect of experimental conditions on nano-indentation response of low-density polyethylene (LDPE)," *Journal of Macromolecular Science, Part A: Pure and Applied Chemistry,* vol. 56, pp. 640–647, 2019.

[61] T. Jin, X. Niu, G. Xiao, Z. Wang, Z. Zhou, et al., "Effects of experimental variables on PMMA nano-indentation measurements," *Polymer Testing,* vol. 41, pp. 1–6, 2015.

[62] G. Arora, and H. Pathak, "Nanoindentation characterization of polymer nanocomposites for elastic and viscoelastic properties: Experimental and mathematical approach," *Composites Part C: Open Access,* vol. 4, p. 100103, 2021.

[63] B.J. Briscoe, L. Fiori, and E. Pelillo, "Nano-indentation of polymeric surfaces," *Journal of Physics D: Applied Physics,* vol. 31, pp. 2395–2405, 1998.

[64] W.C. Oliver, and G.M. Pharr, "Measurement of hardness and elastic modulus by instrumented indentation: Advances in understanding and refinements to methodology," *Journal of Materials Research,* vol. 19, pp. 3-20, 2004.

[65] Q. Kan, W. Yan, G. Kang, and Q. Sun, "Oliver-Pharr indentation method in determining elastic moduli of shape memory alloys - A phase transformable material," *Journal of the Mechanics and Physics of Solids,* vol.61, pp.2015-2033, 2013.

[66] Fischer-Cripps AC. Nanoindentation. Springer New York; 2011.

[67] Y.S. Il, G.E. Gadd, B.A. Latella, V. Lo, R.A. Russell, and P.J. Holden, "Mechanical properties of biodegradable polyhydroxyalkanoates/single wall carbon nanotube nanocomposite films," *Polymer Bulletin*, vol. 61, pp. 267–275, 2008.

[68] M.N. dos Santos, C.V. Opelt, F.H. Lafratta, C.M. Lepienski, S.H. Pezzin, and L.A.F. Coelho, "Thermal and mechanical properties of a nanocomposite of a photocurable epoxy-acrylate resin and multiwalled carbon nanotubes," *Materials Science and Engineering A,* vol. 528, pp. 4318–4324, 2011.

[69] R. Faddoul, N. Reverdy-Bruas, and A. Blayo, "Formulation and screen printing of water based conductive flake silver pastes onto green ceramic tapes for electronic applications," *Materials Science and Engineering B,"* vol. 177, pp. 1053–1066, 2012.

[70] Y. Tang, S. Gong, Y. Chen, LW. Yap, and W. Cheng, "Manufacturable conducting rubber ambers and stretchable conductors from copper nanowire aerogel monoliths," *ACS Nano,* vol. 8, pp. 5707–5714, 2014.

[71] A. Larmagnac, S. Eggenberger, H. Janossy, and J. Vörös, "Stretchable electronics based on Ag-PDMS composites," *Scientific Reports,* vol. 4, pp. 7254, 2014.
[72] D. Doganay, S. Coskun, C. Kaynak, and H.E. Unalan, "Electrical, mechanical and thermal properties of aligned silver nanowire/polylactide nanocomposite films," *Composites Part B: Engineering,* vol. 99, pp. 288–296, 2016.
[73] Y. Kanbur, and U. Tayfun, "Investigating mechanical, thermal, and flammability properties of thermoplastic polyurethane/carbon nanotube composites," *Journal of Thermoplastic Composite Materials,* vol. 31, pp. 1661–1675, 2018.
[74] S. Han Min, A.M. Asrulnizam, M. Atsunori, and M. Mariatti, "Properties of stretchable and flexible strain sensor based on silver/PDMS nanocomposites," *Materials Today: Proceedings,* vol. 17, pp. 616–622, 2019.
[75] H.M. Soe, A. Abd Manaf, A. Matsuda, and M. Jaafar, "Performance of a silver nanoparticles-based polydimethylsiloxane composite strain sensor produced using different fabrication methods," *Sensors and Actuators A: Physical,* vol. 329, pp. 112793, 2021.